International Journal of Pavement Research and Technology
https://doi.org/10.1007/s42947-023-00389-6

社團法人中華鋪面工程學會
Chinese Society of Pavement Engineering

ORIGINAL RESEARCH PAPER

Numerical Modelling and Predicting Performance of Geogrid-Reinforced Low-Volume Unpaved Roads over Soft Subgrades

Boon Tiong Chua[1] · **Kali Prasad Nepal**[2]

Received: 27 May 2023 / Revised: 8 September 2023 / Accepted: 26 September 2023

Abstract
Pavement performance is usually predicted by large-scale laboratory experiments, expensive field tests and/or comparatively cheaper numerical modelling alternative. In this study, a finite element limiting strain model has been developed to investigate the strain response of both unreinforced and geogrid-reinforced pavements on unpaved roads where the geogrid is placed at the bottom of the unbound granular base layer. A two-dimensional (2D) axisymmetric finite element model (FEM) is used to analyse the behaviour of both unreinforced and geogrid-reinforced granular base. The critical pavement responses (vertical surface deformation, compressive strain and compressive stress at the top of subgrade, etc.) are simulated numerically using ABAQUS. These critical responses are used to develop the pavement performance models (strain limiting models) and to predict long-term service life of pavement or the reduction of thickness of granular base for equivalent service life or a combination of both. The parametric results are then used to develop design charts to aid practitioners to use directly in designs. The numerical model is verified using published literature-based information and found to be reasonable. The results show that the traffic benefit ratio (TBR) of 3.1 at a 20 mm rut depth can be achieved for a thin granular base built over soft subgrade using a medium stiff geogrid.

Keywords Pavement performance · Geogrid-reinforced pavements · Finite element model · Traffic benefit ratio

1 Introduction

The use of geogrids to facilitate the construction and to improve the structural performance of low-volume roads over soft subgrades is a common practise in the industry. Geogrid reinforcement is known to increase the composite modulus over 50% in comparison with unreinforced granular base, which implies a substantial saving in pavement thickness or extending the service life of the pavement [1]. The benefits of geogrids in low-volume unpaved roads have been supported by past studies [2–11].

Over the last 4 decades, numerous studies have been undertaken to evaluate the use of geosynthetics for reinforcing granular base. These studies have provided information on the mechanics of the geosynthetics reinforcement, membrane effect of geosynthetics and confinement effect of the base as summarised in Giroud and Noiray [12] and Perkins and Ismeik [13, 14]. Current design practise uses simplified stress distribution models and one or two reinforcement mechanisms with the unpaved pavement structure for large deformation such as methods proposed in Giroud et al. [15], Milligan and Love [16] and Giroud and Han [17, 18]. These methods are generic and assumed a large deformation of permanent unpaved roads.

The geogrid reinforcement is accounted for in the AASHTO design guide for flexible pavements [19]. The design approach involves quantifying the structural contribution of geogrids by the increase of the bearing capacity mobilisation coefficient of the granular base and/or the reduction in the thickness of the base layer. Perkins et al. [20] used FEM to develop the mechanistic–empirical (M–E) modelling of geosynthetics-reinforced flexible pavements based on the unreinforced M–E model [21]. Perkins et al. [22] used the same model to incorporate the influence of

✉ Boon Tiong Chua
boon.chua@kbr.com

[1] Kellogg Brown and Root Pty Ltd, 186 Greenhill Road, Parkside, SA 5063, Australia

[2] School of Engineering, Central Queensland University, 120 Spencer Street, Melbourne, VIC 3000, Australia

Published online: 28 October 2023

pore-water pressure generation in the subgrade. They found that the geosynthetics-reinforced sections are more stable than unreinforced sections.

In Australia, Austroads [23] provides broad coverage on haul road and temporary unbound granular pavements with a focus on geotextiles. Austroads [24] does not provide guidelines on the enhanced stiffness of the geogrid-reinforced granular base layer, rather the geogrid-reinforced granular material is referred to as selected subgrade material. Geogrid reinforcement cannot be modelled directly as a separate layer of the linear elastic model, CIRCLY [25]. By assuming the unreinforced and geogrid-reinforced granular base as selected subgrade, Christopher and Wardle [26] used CIRCLY to determine the pavement thickness of the granular base layer. They found that Austroads [24] approach fails to recognise the improvement by the addition of geogrid reinforcement. This low-risk approach reflects the lack of local performance studies, although there is evidence in the international studies to support the use of geogrids to reduce thickness of the base layer. For the treatment of soft subgrades with California Bearing Ratio (CBR) of less than 3%, DTMR [27] has provided a design table for the suggested granular base working platform wrapped in geotextile and their confinement benefit consideration. RMS [28] has suggested a minimum of 200 mm bound granular base and assumes a subgrade design CBR of 3%. With the exception of DTMR and RMS, other Australasian Road Agencies do not provide additional guidance for subgrade treatment for CBR of less than 3%.

In the UK, the pavement foundation is designed in advance and separately from the pavement structure [29, 30]. This design approach has no perceived benefit and unnecessarily restricts design options. The French method suggests possible treatments by lowering the water table or replacing 500 mm of the soft subgrade or using in situ lime stabilisation [31]. However, there is no method specified to calculate thicknesses using these treatments.

In M–E design, the structural failure is considered primarily due to surface deformation (i.e. rutting). The pavement design approach is to limit the vertical compressive strain at the top of subgrade to a tolerable level throughout its service life. Traditionally, the M–E procedure incorporated the limiting subgrade strain criterion to determine the pavement thickness required to cater for design traffic. There are numerous alternative design methods and their subgrade failure criteria as discussed in Sect. 2. However, a subgrade failure criterion cannot be compared with other in isolation because they are inseparable part of a particular pavement design method.

In this study, an unpaved road pavement damage model (limiting subgrade strain model) has been proposed to limit rutting to less than 20 mm [32]. Considering the fact that it is a small rut, it is reasonable to assume that the resilient strain induced provides an indication of the plastic strain to predict the permanent deformation. This approach allows geogrid to be incorporated into the pavement design using the M–E approach by modifying the limiting subgrade strain equation for rutting to determine the allowable number of traffic repetitions. In this way, contribution of geogrid reinforcement to the structural strength of the pavement can be accounted for using empirical limiting subgrade strain equation for rutting. However, this approach is not currently in Austroads [33] design guide due to lack of local performance studies.

2 Unpaved Road Pavement Performance

Low-volume roads mainly comprise unreinforced or geogrid-reinforced granular materials laid over subgrade. In such pavements, the unreinforced or geogrid-reinforced granular material is the main structural layer to carry the traffic load. The structural performance for this type of pavement is dictated primarily by rutting or loss of surface shape attributed to the compressive vertical compressive strain at the top of the subgrade. A common damage model (transfer function or failure criteria) used to define the relationship between the limiting vertical compressive strain on the subgrade and the number of standard axle load repetitions to cause failure by excessive rutting has been used extensively in M–E design of flexible pavements [25, 34, 35]. Past researchers [36, 37] used AASHTO road test data to develop their subgrade strain criterion and found the strain instead of stress criterion is independent of the subgrade stiffness. Dorman [38] evaluated the design charts and found that the allowable vertical compressive strain at the top of the subgrade was practically a constant irrespective of the pavement thickness. The allowable vertical compressive stress for design is a function of the subgrade CBR but it does not depend on the number of load repetitions. It is for this reason, the theory of vertical stress criteria proposed by Peattie [39] never caught on.

Past researchers and several agencies [22, 33, 37, 40–54] have used a power model as shown in Eq. (1) to relate vertical compressive strain at the top of the subgrade (ε_v) to the allowable number of traffic load (N) before an unacceptable level of pavement surface deformation develops.

$$N = \left[\frac{k}{\varepsilon_v}\right]^B, \tag{1}$$

where k is the material constant, B is the damage exponent and ε_v is the induced vertical compressive strain (in terms of microstrain) at the top of the subgrade.

Historically, the vertical compressive strain is estimated by layered-elastic analysis [33]. This approach assumes that the permanent strain is proportional to elastic strain [55].

By limiting the elastic strain to some prescribed value also limits the plastic strain. The integration of the permanent strain over the depth of the pavement structure provides an indication of the rut depth. Therefore, by limiting the elastic strain at the top of the subgrade, the magnitude of the rut is controlled. Table 1 summarises different values of coefficients for the subgrade failure in Eq. (1) used by different agencies and research literatures.

The empirical power model in Eq. (1) is used to determine the pavement thickness required to cater for the design traffic. Each failure criterion is an inseparable part of a specific pavement design method, which implies that it cannot be extracted and applied outside the context it was developed. When the limiting subgrade vertical compressive strain is analysed for both unreinforced and geogrid-reinforced granular base for the same pavement structure and for a specified rut depth, the ratio N_R (allowable traffic loading for geogrid-reinforced pavement) over N_{UR} (allowable traffic loading for unreinforced pavement) is equal to traffic benefit ratio (TBR). By substituting Eq. (1), the relationship between TBR and subgrade strains can be developed and presented in Eq. (2).

$$\mathrm{TBR} = \frac{N_R}{N_{\mathrm{UR}}} = \left[\frac{\varepsilon_{v-R}}{\varepsilon_{v-\mathrm{UR}}}\right]^{-B}, \tag{2}$$

where the symbols UR and R denote unreinforced and geogrid-reinforced granular base.

3 Problem Statement and Study Objective

Although the basic functions of geogrid-reinforced granular base are reasonably understood by road agencies to extend the service life of pavement, to reduce pavement thickness for equivalent service life, or a combination of the two, there is no guidelines for designers. The literature review revealed that there is no known rutting model for geogrid-reinforced granular base on soft subgrade soils with CBR of 3% or less. The objective of this study is to develop a limiting subgrade strain criterion (damage model) and to produce pavement design chart for low-volume unpaved roads on soft subgrade with geogrid-reinforced granular base. The work performed in this study addresses the use of geogrid reinforcement in conjunction with the design by the M–E procedure.

4 Finite Element Modelling

Though three-dimensional (3D) model can better replicate the actual tyre imprint of the wheel load on the pavement structure than the circular loaded area as restricted in two-dimensional (2D) axisymmetric analysis or the infinite strip load as in 2D plane strain analysis, it requires more computational time and computer memory. It is time-consuming and not practical to run multiple cases for parametric studies. The 2D axisymmetric model is known for its simplicity, greater efficiency regarding computation time, reduction of data and adaptability to pavement models with more cost-effective solutions than 3D modelling. As such, a 2D axisymmetric model is developed in ABAQUS to analyse the two-layer soil system for both with and without geogrid reinforcement of granular base. This approach is consistent with the past studies [9, 63–67].

4.1 Model Geometry

The accuracy of computational results is dependent on the model's geometry [9]. Several past studies have used varying model geometry and defined the domain size using equivalent radius (r) of the circular loaded area as summarised in Table 2.

The dimensions of the axisymmetric model in this study are selected in such a way that the effect of load dissipation is contained to control the computational time. If the maximum induced stress at the outer boundary is less than 0.01% of the applied contact pressure, then it can be considered negligible [72] and acceptable in pavement design practise. In addition, the model dimensions are selected to minimise the undesirable resonance effects of the boundary's reflection. Kim et al. [74] found that the FEM results are in good agreement with KENLAYER results when adopting 140 times the radius in the vertical and 20 times the radius in the horizontal dimension. The final adopted FEM dimensions are 2.3 m radius cylinder with 0.2 to 0.8 m thick granular base on 12.75 m soft soil to replicate infinite depth as illustrated in Fig. 1. This equates to approximately 25 times and 145 times the radius of circular loaded area for the model radius and height, respectively, to represent the outer model boundaries. As the pavement model is axisymmetric, only half of the whole system is modelled.

4.2 Boundary Conditions

The conventional kinematic boundary conditions are adopted in this study whereby boundaries are assigned to the outer perimeter, the rotation axis and the bottom of the model. However, the top surface of the model is unrestrained and the outer perimeter is restrained in the radial direction but allowed to move in the vertical direction. The bottom of the model is assumed to be encastred (fixed) and restrained from moving both vertically and horizontally.

Table 1 Rutting model coefficients

Agency/researcher	k	B	Comments
Heukelom and Klomp [40]	5405	7.09	Model coefficients derived from power trendline based on $\varepsilon = [10]^{-A}$ where $A = 0.1408\log_{10}N_i + 2.408$
Dorman and Metcalf [37]	10,556	4.98	Based on AASHTO road test with relatively thick asphalt surfacings subject to freeze–thaw cycle, tyre pressure 550 kPa, radius 150 mm, silty clay (A-6) subgrade, rut depth 19 mm,
Monismith and McLean [41]	11,025	4.35	Rut depth 7.5 mm
Shell [43]	28,000	4	50% reliability, based on AASHTO road test and Dorman and Edwards [36] study
Shell [44]	18,000	4	Adopted in DESIGNPAVE CMAA software (Rahman et al. [58]) 95% reliability, based on AASHTO road test
Brown and Brunton [42]	21,600	3.57	British conditions for UK practise Road Note 29, rut depth 20 mm
US Army Corps of Engineers (Barker and Brabston [45])	5525	6.527	50% reliability, aircraft test pavement
British Airports Authority (Woodman [46])	5820	5.747	50% reliability, based on USACE aircraft test pavement
DoA (Chou [47])	4352	6.897	Based on subgrade CBR 7–10%, military roads and elastic layered method. $N = 10^A$ where $A = -(2.408 + \log \varepsilon_v)/0.1408$
UK Transport and Road Research Laboratory [48]	25,951	3.75	UK Road Note 31, applicable to tropical and sub-tropical road conditions with 20 mm rut depth
New Zealand (Pidwerbesky [49])	21,000	4.348	Primary highways
	25,000	4.348	Secondary highways
			New Zealand agency has adopted Austroads [33] limiting subgrade failure criteria and Austroads CBR design chart Figures 8.4 and 12.2
French Method (Corte and Goux [50])	16,000	4.505	
Wardle and Rodway [51]	4276	6.635	50% reliability, based on USACE aircraft test pavement
Asphalt Institute [56]	17,509	4.477	Tyre pressure 689 kPa over 96.01 mm radius
Wardle et al. [57]	k	B	Based on USACE CBR method (S77-1 Method, Pereira [59]) calibrated with aircraft loading. HIPAVE [35] adopted this failure criterion model
			$k = 1.64\times10^{-09}E^3 - 4.31\times10^{-07}E^2 + 2.18\text{X}10^{-05}E + 0.00289$
			$B = -2.12\times10^{-07}E^3 + 8.38\times10^{-04}E^2 - 0.0274E + 9.57$
Road Belgian Research Centre (Huang [52])	11,025	4.35	Based on Monismith and McLean [41]
Indian Road Congress [53]	23,557	4.5337	80% reliability, axle load 81.6 kN, rut depth 20 mm
Perkins et al. [22]	22,323	4.292	Model coefficients derived from power trendline based on $\delta = \xi_1 A e^{-\left(\frac{\rho}{N}\right)^{\xi_2\beta}} \varepsilon_v h$ where δ is rut depth, N is traffic repetitions, A, β, ρ are material properties, ε_v is vertical strain, h is layer thickness, ξ_1, ξ_2 are field calibration coefficients. Based on Georgia subgrade, 550 kPa pressure over 152 mm radius
Austroads [60]	8511	7.14	CBR design chart—Figures 8.4, tyre pressure 550 kPa, radius 110 mm, N unit in Standard Axle Repetitions (SAR), 20 mm rut depth
Austroads [61]	9300	7	CBR design chart—Figures 8.4 and 12.2 in Austroads Part 2, tyre pressure 750 kPa, radius 92.1 mm, N in SAR unit, 20 mm rut depth
Austroads [33]	9150	7	CBR design chart—Figures 8.4 and 12.2 in Austroads Part 2, tyre pressure 750 kPa, radius 92.1 mm, N in ESA unit, 20 mm rut depth
			CIRCLY [25] used the same failure criterion
Gupta et al. [54]	5000	6.024	Nonlinearity in granular layer, rut depth 25 mm
Gupta et al. [54]	5800	5.848	Nonlinearity in granular and subgrade, rut depth 25 mm
Vern et al. [62]	70,000	2.89	Silty-clay and silty-sand only, 25 mm rut depth
	250,000	2.89	Clay only, 25 mm rut depth
			Used Boussinesq equations and assumed isotropic soil

Table 2 Studies on model geometry

References	Model radius (times r)	Model height (times r)	Comments
Duncan et al. [68]	12	50	Unreinforced 2D axisymmetric FEM
Helwany et al. [65]	6	6.25	Unreinforced 2D axisymmetric FEM
Perkins [69]	6.6	10	Reinforced 3D FEM
Perkins and Edens [70]	6.6	10	Reinforced 3D FEM
Leng and Gabr [7]	4.9	5.9	Reinforced 2D axisymmetric FEM
Saad et al. [71]	14	14	Reinforced 3D FEM
Howard and Warren [66]	20	30	Reinforced 2D axisymmetric FEM
Abu-Farsakh and Nazzal [72]	29.6	26.3	Reinforced 2D axisymmetric FEM
Moayedi et al. [73]	20	10	Reinforced 2D axisymmetric FEM
Kim et al. [74]	20	140	Reinforced 2D axisymmetric and 3D FEM
Sahoo and Reddy [75]	9	12	Unreinforced 3D FEM
Gu [76]	29.6	26.3	Reinforced 2D axisymmetric FEM
Austroads [77]	25	32	Reinforced 2D axisymmetric FEM
Pandey et al. [78]	25	35	Reinforced 2D axisymmetric FEM
Ghadimi et al. [79]	55.55	166.7	Unreinforced 2D axisymmetric FEM
Kim and Lee [80]	20	140	Reinforced 3D FEM
Abu-Farsakh et al. [9]	29.6	26.3	Reinforced 2D axisymmetric FEM
Faheem and Hassam [81]	15	10	Reinforced 2D axisymmetric FEM
Al-Jumaili [82]	10	20	Reinforced 3D FEM
Samb et al. [83]	12	18	Unreinforced 2D axisymmetric FEM
This study (2023)	25	145	Reinforced 2D axisymmetric FEM

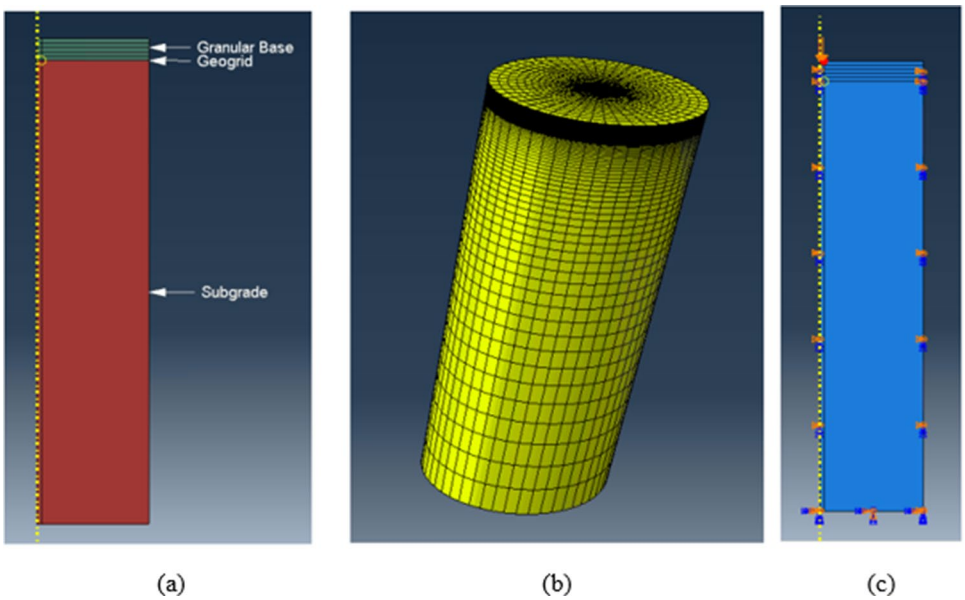

Fig. 1 **a** 2D axisymmetric pavement model, **b** FEM mesh, **c** boundary conditions and load

4.3 Traffic Loading

The FEM model in this study is for simulating single axle dual tyre (SADT) applying a load of 80 kN including the gravity load in the initial loading step of the analysis. The axle load is simulated by applying the contact pressure of 750 kPa on a circular area with a radius of 92.1 mm at the surface [33]. A haversine-shaped load wave of 0.1 s [84–86] with the maximum magnitude of 20 kN is adopted to simulate a single wheel load of a standard axle. The cyclic loading is implemented into ABAQUS with the help of subroutine DLOAD. However, as 2D axisymmetric model can only replicate a single circular load, it is not possible in this geometrical formulation to handle dual tyres or multiple axles

loading conditions. Considering the compressive strain on top of the subgrade is very small and the surface deformations are recoverable under repeated application of traffic loads, it is reasonable to assume the pavement model performance is within the elastic range. Linearity implies the applicability of the superposition principle. Huang [52] used this technique to develop strain conversion factor charts to determine the strain factor for dual wheels. Australia [77] proposed a simplified superimposing method and successfully used in the finite element study as illustrated in Fig. 2. In this study, Austroads [77] method is adopted for simplicity.

The modelling of multiple circular loads such as SADT is performed by superimposing the single load prediction responses at various offsets [77]. Standard axle loading consists of a dual tyred single axle, applying a 80 kN load and with circular tyre contact stress of 750 kPa. The four-wheel loads are numbered from 1 to 4 as shown in Fig. 2. The critical response within the pavement is assumed to occur along the vertical axis located symmetrically between a pair of dual wheels, at the top of the subgrade. Therefore, the effect of the four loads at the centre of inner wheel is accounted for by adding all the strains obtained from each load. It should be noted that the superposition of stresses and strains occurs at the end of the numerical analysis.

4.4 Finite Element Type

Eight-node biquadratic axisymmetric quadrilateral solid elements (CAX8R) are used to discretise the granular base and subgrade, whilst two-node linear axisymmetric membrane elements (MAX1) with the thickness of 3 mm are used to discretise the geogrid reinforcement [87]. A finer mesh near the surface wheel load is used to capture the steep stress and strain gradient within this area. By implementing edge biassed structural meshing pattern in ABAQUS, a smooth transition from finer mesh at the loaded area to coarser mesh in the region away from the loading area. The same mesh pattern is used to simulate all layers to preserve the continuity of nodes between consecutive layers. The optimum number of finite elements meshes for the FEM is determined by trial and error with the mesh sensitivity tests until the numerical analysis converges to a unique solution.

4.5 Materials

The modulus of unbound granular materials and subgrade are dependent on the stress level at which they operate and the modulus of the underlying layers. This infers that the modulus of granular material decreases with depth and is influenced by the modulus of the subgrade. Mohr–Coulomb elastoplastic models are selected to represent the nonlinear material properties whereby the shear strength developed is a function of internal friction, cohesion and applied stress. The granular base is assumed to be purely frictional granular soil. But to enhance the stability of numerical analysis, the cohesion for granular base is set as 0.1 kPa [88, 89]. Past researchers have successfully used Mohr–Coulomb elastoplastic model [7, 67, 90].

For simplicity, Austroads [33] sub-layering approach is used to replicate the cross-anisotropic characteristics of subgrade and granular base. Khodakarami and Moghaddam

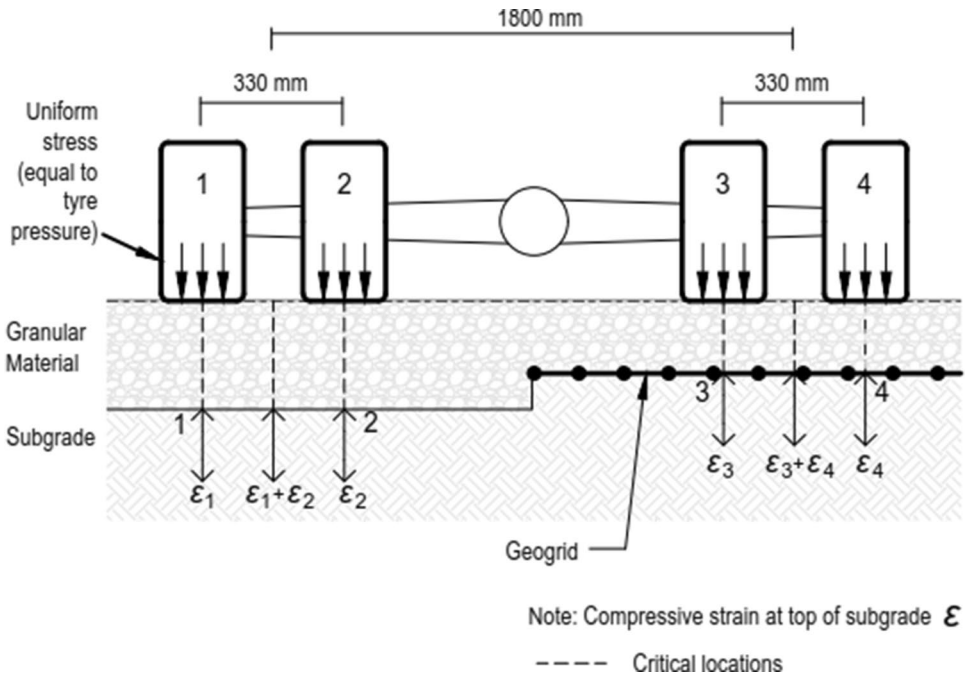

Fig. 2 Superposition of strains in axisymmetric model (adapted from Austroads [77])

[91] used the sub-layering technique to study the performance of geogrid-reinforced in rehabilitated paved roads by 2D FEM models. This approach assumes that the modulus of unbound granular base layer varies with the underlying subgrade support with CBR ≥ 3%, which better reflects in-service performance to estimate the average resilient modulus. However, soft subgrade materials with CBR < 3% are unlikely to behave elastically when loaded [27]. This is attributed to the fact that soft subgrade does not provide a stable working platform required to obtain good compaction of the granular layer, thereby resulting in lower modulus value. This approach prevents the use of maximum modulus of a granular material to be developed regardless of the thickness of the granular layer or the underlying subgrade strength. Under this condition, the modulus ratio of granular to subgrade is usually taken to be 1 to 5 as recommended by Heukelom and Klomp [40] and a ratio of 2 to 5 are selected in this study. A band of modulus values of granular base corresponds to lower and upper bound subgrade support values, respectively, shown in Table 3. In addition, other presumptive material input parameters used in this study are based on published data [33, 92, 93].

Past researchers have found that the influence of the associated flow rule is significant for higher friction angle ($\phi > 30°$) up to 15% [90, 94, 95]. Soil dilatancy is accounted for in Mohr–Coulomb model by allowing the yield surface to expand based on plastic straining. In this study, the associated flow rule is replicated by selecting the dilatancy angle ψ equal to internal friction angle less than 30° [89, 93, 96].

4.6 Geogrid-Reinforced Pavement Model

For the condition of a small rut of less than 20 mm, the induced strain in the geogrid is very small and is considered within the elastic range. Hence, a linear elastic model is used to describe the behaviour of geogrid material. In addition, the maximum geogrid tensile strength (axial stiffness) at 2% strain from the material in the machine and cross-machine directions is used. This means that the direction-dependent character of the geogrid is not considered for simplification. Other researchers have successfully used the same modelling assumption [11, 69, 97, 98]. The mechanical stabilising effect of geogrid extends over 100 mm from the geogrid plane and is simulated in the model by assigning stress concentrations of 63 kPa at the geogrid elevation and decreases linearly at a constant rate to nominal 21 kPa at 100 mm above the geogrid plane within the influence zone [9, 99]. The medium stiff geogrid is selected for this study because it is commonly used in engineering practise.

The soil–geogrid interface model is implemented by adopting the ABAQUS contact interaction feature. This feature entails one surface acting as a rigid body. This is defined as a 'master' surface and the other deformable body surface provides the 'slave' surface. Under this arrangement, the nodes on the slave surface are constrained not to penetrate to the master surface and the nodes of the master surface can, in principle, penetrate into the slave surface. Once the contact pair is defined, the programme automatically generates a family of contact elements. The clearance and relative shear sliding for these elements are measured at each integration point. These kinematic measures are then used, together with the appropriate penalty friction formulation techniques to introduce surface interaction theories.

In the unreinforced case, the interface between granular base and subgrade is assumed to be fully bonded using surface-based tie constraint with node-to-surface instead of surface-to-surface formulation. The surface-to-surface formulation cannot accommodate a mixture of rigid and deformable portions of a surface. This restriction is overcome with the adoption of node-to-surface formulation. For geogrid-reinforced case, the granular base–geogrid–subgrade interface is assumed to be kinematic coupling constraints using node–node formulation with a reference node. This approach will ensure that the geogrid is held in place at the interface when the model is in motion under the applied load.

The geogrid is simplified as continuous membrane embedded between the granular base and subgrade. With the assumption of continuity for geogrid in the finite element model, it is not feasible to directly simulate the interlocking

Table 3 Material properties for FEM analysis

Materials	Element (type)	Model and parameters	Thickness (mm)	Modulus (MPa)	Poisson ratio (ν)	Comments
Granular base	Solid (CPE8R)	Mohr–Coulomb $\phi = 40°$ $c' = 0.1$ kPa	300–800	20–300	0.35	Dense granular base
Subgrade	Solid (CPE8R)	Mohr–Coulomb $\phi = 0°$ $c_u = 30$–90 kPa	12,750[a]	10–30	0.45	Very soft to stiff soil (clay)
Geogrid	Membrane (MAX1)	Elastic	3	500	0.35	Medium stiff geogrid

Material parameters based on compilation of published data from Look [92], Ameratunga et al. [93] and Austroads [33]

[a]Denotes infinite depth

between the geogrid and surrounding pavement materials. This is addressed using Coulomb friction model to simulate the shear resistance interaction at the interface between the geogrid and pavement materials [80, 100–102]. This is implemented using the friction coefficient of the interfaces μ and the elastic slip input data into ABAQUS. An elastic slip of 0.001 m is adopted based on Perkins and Cuelho [103] and Perkins [69]. The friction coefficients of geogrid-granular base of 0.84 and geogrid-subgrade of 0.62 have been selected for this study based on BOSTD [104].

5 Verification of Finite Element Model

For model verification, the same granular base thickness and material properties used by Leng and Gabr [7] are adopted. Prior to parametric study, the FEM results are validated with published results of Leng and Gabr [7]. The vertical stress distribution underneath the centre of the uniformly loaded circular area through the granular base and subgrade layers is shown in Fig. 3. The stress distribution is not smooth for the elastoplastic FEM at the interface of granular base–subgrade as compared with linear elastic model as in KENLAYER programme and Boussinesq's homogeneous elastic solution. This is attributed to shear resistance interfaces and is more pronounced when the geogrid-reinforced granular base becomes stiffer owing to tensile resistance and limit tensile yielding at the bottom of the granular base layer resulting in lower vertical stress in the granular base layer.

The effect of material characteristics can be seen in Fig. 3a. KENLAYER and Boussinesq's elastic models are stiffer pavement system (constant elastic modulus) with lower vertical stress for depths greater than 0.4 m in the subgrade layer. In all cases, the elastoplastic FEM predicted lower vertical stress in the granular base layer which is more pronounced with geogrid reinforcement.

The vertical strain distribution through the granular base and subgrade layers along the centreline of the loading area is shown in Fig. 3b. The results show that there is a large vertical strain at the bottom of the unreinforced granular base layer resulting from yielding of the granular layer due to low tensile strength causing the outward lateral spreading of the granular base material. It also shows that the vertical strains at the bottom of granular base are significantly reduced when geogrid reinforcement is included. These results illustrate the geogrid reinforcement ability to limit lateral spreading of granular base and is fundamentally linked to the stress response of the pavement structure.

Overall, the vertical stress and strain results from this study show good agreement with elastoplastic FEM analysis conducted by Leng and Gabr [7].

6 Results and Discussion

6.1 Design Equations and Curves

Empirical design chart by Austroads [24] for lightly trafficked roads is used to determine the thickness of unreinforced granular base for five sets of traffic loading (i.e. 1×10^3, 5×10^3, 1×10^4, 5×10^4 and 1×10^5 ESA) and repeated for six sets of subgrades CBR values (2, 3, 4, 5, 6 and 7%). The results show a linear relationship between the thickness (H) of unreinforced granular base and the design traffic (N) for each subgrade CBR value as depicted in Fig. 4.

When the data points are fitted with a semi-log trend line for each subgrade CBR value, it shows a distinctive semi-log equation form as in Eq. (3).

$$H = A \ln N + B, \tag{3}$$

where A and B are parameters determined from each curve in Fig. 4.

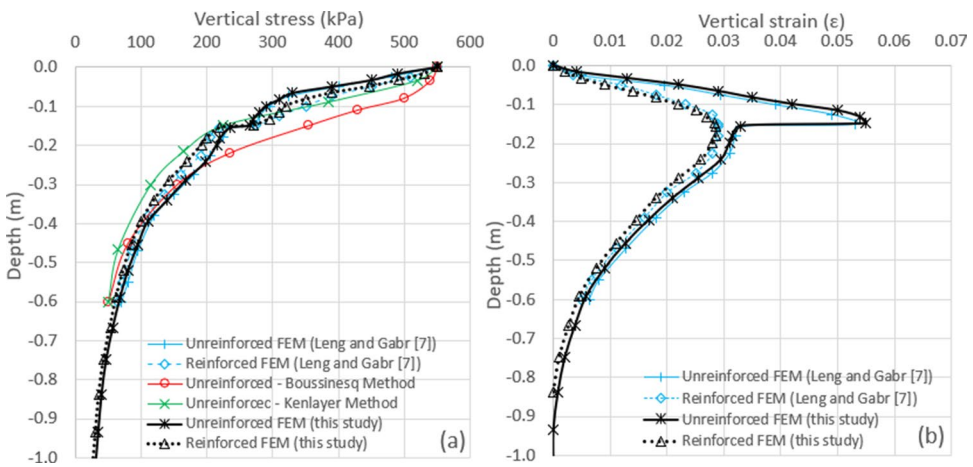

Fig. 3 Comparison of vertical stress and stain results based on $H_{base}=0.15$ m, $E_{base}=50$ MPa, $E_{subgrade}=10$ MPa, $E_{geogrid}=100$ MPa (Data source: Leng and Gabr [7])

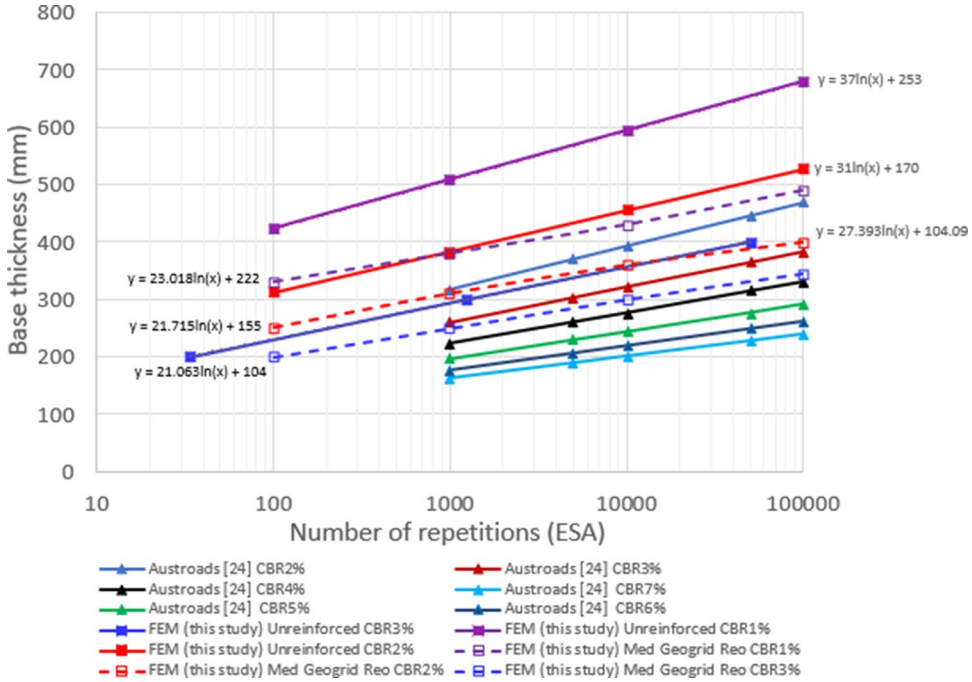

Fig. 4 Granular base versus number of repetitions

This process was repeated for unreinforced granular base with internal friction angle $\phi = 40°$. The granular material is similar to normal crushed rock base quality material. The results from this seem to be more conservative when compared with Austroads [24]. This is attributed to the nonlinear constitutive model being used in FEM.

The parameters A and B determined from each curve for subgrade CBR of 1, 2 and 3% were then plotted against the subgrade CBR and used the polynomial trend line to establish the good fit to the data as shown in Fig. 5.

The regression equations for A and B obtained for the curve are used in conjunction with Eq. (3) to derive design curves, and hence to determine thickness of granular base. Similar approach is followed for medium stiff geogrid-reinforced granular base with internal friction angle $(\phi) = 40°$. The regression equations for unreinforced granular base are presented in Eqs. (4) and (5).

$$A = 1.1965\text{CBR}^2 - 9.5895\text{CBR} + 45.393 \tag{4}$$

$$B = 8.545\text{CBR}^2 - 101.65\text{CBR} + 353.09 \tag{5}$$

The equations for medium stiff geogrid-reinforced granular base are in Eqs. (6) and (7).

$$A = 0.3255\text{CBR}^2 - 2.2795\text{CBR} + 24.972 \tag{6}$$

$$B = 8\text{CBR}^2 - 91\text{CBR} + 305 \tag{7}$$

where A and B are regression function parameters relating to subgrade CBR values. These equations are valid for

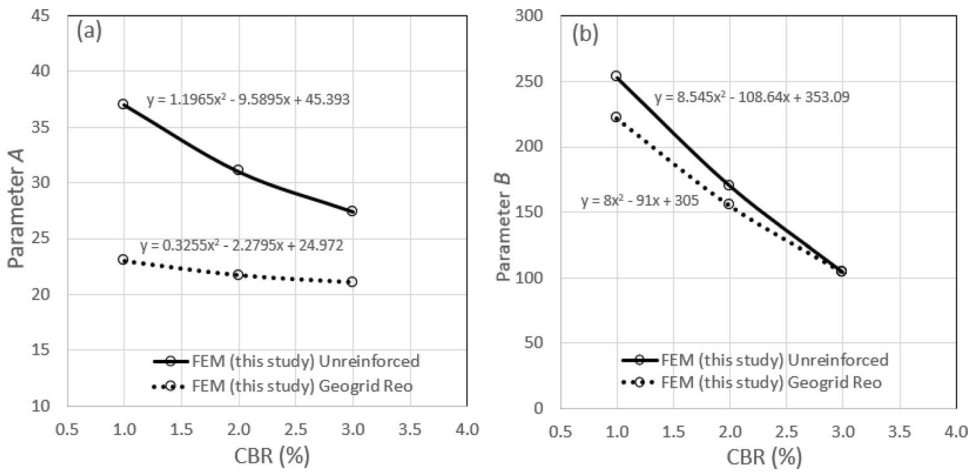

Fig. 5 **a** A versus subgrade CBR **b** B versus subgrade CBR

low-volume roads with subgrade CBR less than or equal to 3%.

6.2 Comparison with Other Methods

The thickness of pavement with and without a geogrid reinforcement obtained from the proposed design equations is used to compare with other established methods. For unreinforced granular base over subgrade CBR of 3% and 2%, the design curve obtained from this study shows close agreement with mechanistic–empirical method using CIRCLY programme as shown in Figs. 6a and b. When compared with Austroads [24] and AASHTO [19], the design curve is bounded by these two methods with the similar trend. The proposed design curve underestimates the base thickness in comparison with the Giroud and Han (G–H) [17, 18], whereas Holz et al. [105] method is comparable for number of repetitions less than 10^3 ESA. The commonly used Road Note 31 [48] empirical approach widely used in tropical and sub-tropical countries appears to underestimate the thickness of pavement and is more applicable to traffic exceeding 3×10^6 ESA. In the case of subgrade CBR 3%, South Africa Method [106], Indian Road Congress [107] and ARRB [108] approach appear to have a leaner design. This could be attributed to low reliability level of 50 to 80% being used. HIPAVE [35] method is overly conservative for standard axle loading and is applicable to higher loadings condition used at ports and container terminals [109]. The failure model for HIPAVE [35] is based on USACE CBR method [59] calibrated with aircraft loading. Figure 6a and b clearly shows that the use of HIPAVE method is not applicable to standard axle loading condition. For soft subgrade with CBR less than 3%, the DTMR [27] empirical method appears overly conservative when compared with all other methods as shown in Fig. 6b and c.

For geogrid-reinforced base over subgrade CBR of 3% and 2%, the pavement thickness obtained from this study shows good agreement with Holz et al. [105] and Giroud and Han [17, 18] methods as shown in Fig. 7a and b. In all cases, Perkin [110] empirical method shows similar trend but appears to underestimate when compared with other methods including the proposed design curves. For

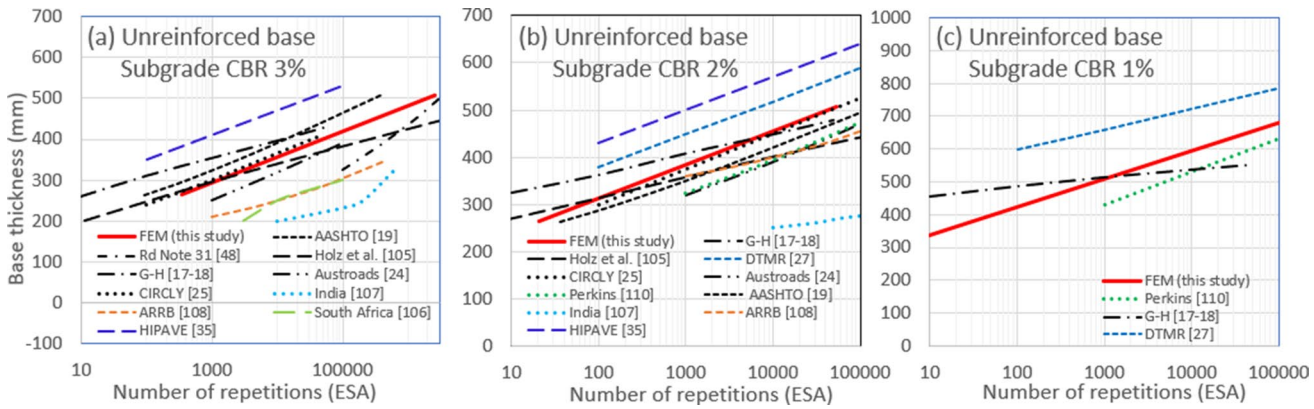

Fig. 6 Comparison of pavement thickness with other approaches for unreinforced base

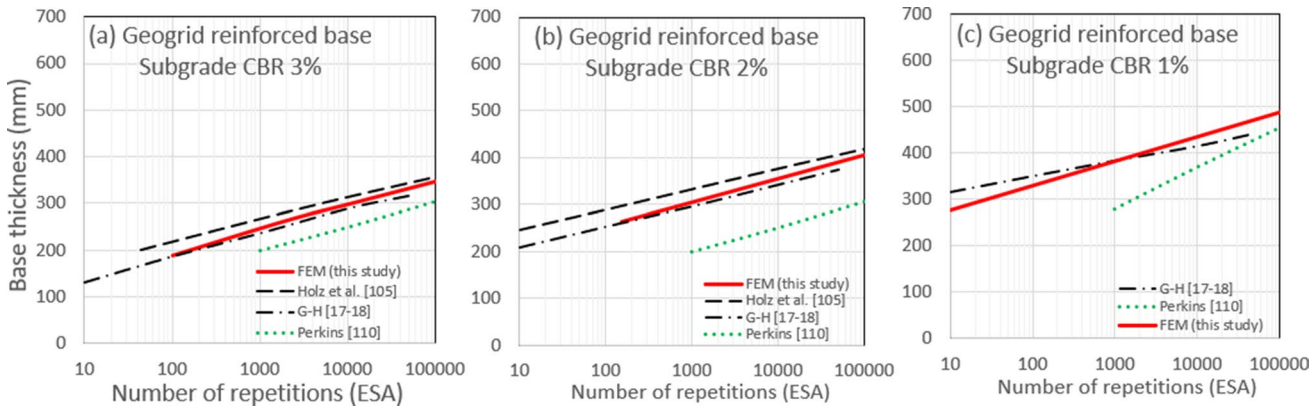

Fig. 7 Comparison of pavement thickness with other approaches for geogrid-reinforced base

soft subgrade CBR 1% as shown in Fig. 7c, there is slight deviation in trend with increase in number of repetitions exceeding 10^3 ESA. This could be attributed to the unstable nature of the models for very weak soil conditions.

It is evident from this study, that the pavement thickness on soft subgrade soil using the proposed design curve derived from the proposed design equations is comparable with the established methods.

6.3 Limiting Subgrade Strain Curves

A common damage model used to define the relationship between the limiting vertical compressive strain on the subgrade and the number of standard axle repetitions to cause failure by excessive rutting has been extensively used in M–E design of flexible pavements [25, 34, 35]. In this study, results from FEM for 20 mm rut depth for both unreinforced and geogrid-reinforced granular bases over soft subgrade are fitted with power trend lines as shown in Fig. 8.

Figure 8 shows that the vertical compressive strain at the top of subgrade decreases with the increase in the number of load repetitions. For a given number of load repetition, the allowable subgrade strain is consistently higher for the geogrid-reinforced granular base case as compared to the unreinforced case similar to a shifted line for reinforced granular base. This implies that for a given subgrade strain value geogrid reinforced granular base case has higher number of repetitions as compared to unreinforced case. Based on the FEM results, this study proposes the following limiting subgrade strain criterion

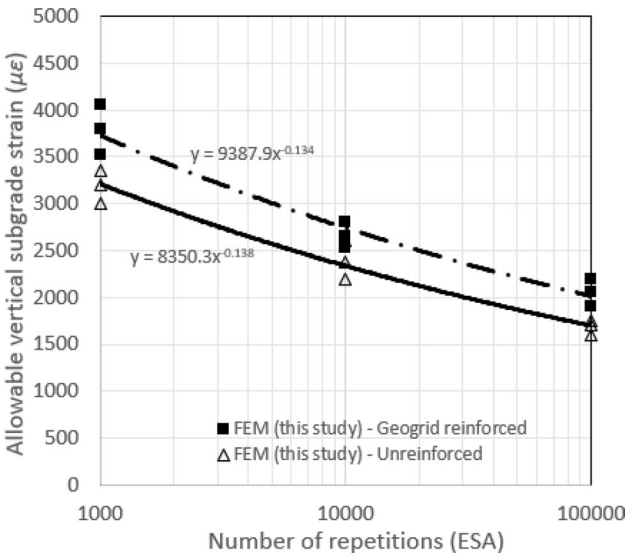

Fig. 8 Maximum allowable subgrade strain criterion

for unreinforced and medium geogrid-reinforced granular base for low-volume roads:

$$N_{\mathrm{UR}} = \left(\frac{8350}{\mu\varepsilon}\right)^{7.2} \tag{8}$$

$$N_R = \left(\frac{9388}{\mu\varepsilon}\right)^{7.5}, \tag{9}$$

where N_{UR} and N_R are allowable number of standard axle load repetitions for unreinforced and geogrid-reinforced granular base, respectively.

The validity of these damage models is checked by comparing with the results from established methods [22, 33, 43, 50, 53, 56] and results are shown in Fig. 9.

The proposed subgrade strain line is comparable with Austroads [33], Shell [43], French Design Method (Corte and Goux [50]), Indian Road Congress [53] and Perkins et al. [22]. The lower allowable strain line developed by Brown and Brunton [42] assumes a greater proportion of permanent deformation in the asphalt, which is more appropriate for full-depth asphalt pavements and British conditions whereas, Asphalt Institute [56] line relates to climatic conditions of California. Shell [43, 44] and Brown and Brunton [42] developed their curves from the observed performance of in-service roads subjected to truck loadings with dual tyre up to around 5 tonnes. Shell [43, 44] lines are derived from the AASHTO road test with the strong influence of the freeze–thaw cycle appropriate to Illinois. However, the use of AASHTO data to derive limiting subgrade strain criterion need to be used with caution. It is based exclusively on the silty clay soil at one moisture content and may not be applicable for other materials (gravel, sand, silt, or clay) nor for other moisture conditions. In addition, the use of elastic parameter such as subgrade strain to predict a plastic deformation may not be a rational approach. Furthermore, the estimates of the limiting strain effects were based on relatively thick asphalt surfacing which were subject to freeze–thaw cycles not applicable to bulk of Australian road network conditions.

The study by Perkins et al. [22] is based on Georgia subgrade which is appropriate for American conditions. Based on large field performance data of bituminous pavement across India under various climatic conditions, Indian Road Congress [53] specifies the rutting life relationships for subcontinental conditions. However, all the subgrade criteria assume that the granular base has no influence on pavement performance. It assumes that the pavement as a whole may rut by idealising the subgrade deforming with the granular base deflecting bodily on it without thinning, meaning that the permanent deformation for the granular base layer is not included in the procedure. To the best of authors'

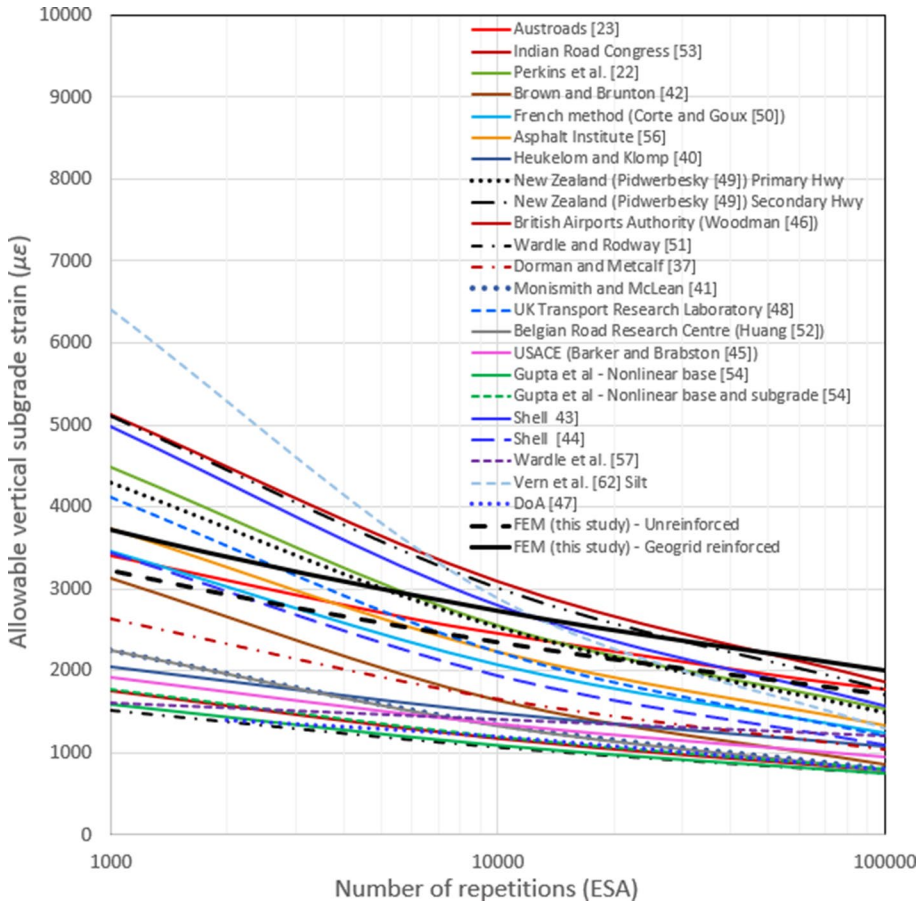

Fig. 9 Comparison of maximum allowable subgrade strain criteria

knowledge, there is no suitable model to reliably predict the rutting in granular base layer under traffic [24]. In the case of reinforced granular base, there are no published literatures available for benchmarking as evident in Fig. 9 where all the published data are for unreinforced granular base.

The damage models in Eqs. (8) and (9) can be incorporated into the M–E framework to evaluate the strain (ε_v) at the top of the subgrade for a given pavement structure to estimate the number of traffic passes with and without geogrid-reinforced granular base and the TBR value. Using this approach, the benefit of geogrid reinforcement can be quantified. For the same subgrade strain value, the ratio of N_R over N_{UR} is equal to TBR. Based on Eq. (2), the proposed limiting subgrade strain criterion for unreinforced and geogrid-reinforced granular base, the estimated TBR at 20 mm rut depth for medium stiff geogrid reinforcement is approximately 3.1. This result is comparable with TBR results at 25 mm rut ranges from 1.6 to 4.1 obtained by Cuelho et al. [111]. Based on Cuelho et al. [111], it can be inferred that higher allowable rut will lead to higher TBR values. It should be mentioned that the proposed equations are validated by a relatively small database and it is important to further verify using field tests on actual full-scale geogrid-reinforced granular base pavements in the future.

6.4 Limitations and Applicability

The pavement design curves and the limiting subgrade strain curves (and associated equations) developed in this study are valid only for a set of specific conditions. First, the subgrade is assumed to be saturated with low permeability and it behaves in an undrained manner under traffic loading. Second, the design curves are valid for the number of allowable traffic loads not exceeding 10^5 ESA for a terminal rut depth of less than 20 mm. Third, there is no allowance for the effects of dynamic loading factor to account for cornering, acceleration, braking and surface unevenness. Forth, these design curves only apply to medium stiff geogrids laid on a horizontal plane at the interface of granular base and subgrade. Fifth, the design curves assume that the granular base is a normal standard crushed rock (CBR $\geq$ 80%) commonly used by road agencies [24]. Sixth, the geogrids should meet the minimum standard specification as per DTMR [112] or AASHTO [113]. Seventh, single axle with dual tyres (SADT) applying a load of 80 kN and uniformly loaded circular areas of equal area (radius 92.1 mm) with tyre contact stress of 750 kPa is used to develop equations and curves. Eighth, the simulated maximum vehicle speed is 50 km/h [114].

Ninth, each layer is homogeneous with a finite thickness, except that the subgrade layer is infinite in thickness. Lastly, the curves should not be extrapolated beyond the data base used to develop them.

7 Conclusion and Recommendations

An M–E pavement design approach for geogrid-reinforced granular base on low-volume unpaved roads has been developed using a 2D axisymmetric finite element model. The objective of this paper is to analyse the critical responses of the pavement layers and to establish limiting subgrade strain models that relates to long-term pavement performance or the reduction of granular base layer thickness for equivalent service life or a combination of both. This approach allows to incorporate geogrid reinforcement in the M–E pavement design method by modifying the limiting subgrade strain equations for rutting and to determine the allowable number of traffic repetitions (service life). The contribution of geogrid reinforcement to the pavement structural strength can also be quantified. The proposed regression equations can be used in lieu of design curves to determine the thickness of the granular base. The limiting subgrade strain equations for unreinforced and geogrid-reinforced granular base can be used to determine the TBR. The FEM results show that the TBR value of 3.1 at 20 mm rut depth can be achieved for thin granular base built over soft subgrade using medium stiff geogrid. However, the proposed regression equations are appropriate to a locality that is dependent on the performance of granular base, subgrade and geogrid that were used to develop the FEM. The developed failure criterion is an inseparable part of the design curves, which means it cannot be directly used to compare with other methods in isolation.

Acknowledgements The facilities for conducting this study provided by La Trobe University is gratefully acknowledged. The authors are responsible for the opinion expressed in this paper.

Author Contributions BTC: This manuscript was prepared as part of PhD research project at La Trobe University. Boon performed the finite element analysis, interpreted and compiled the results. Boon is the primary author of this manuscript and will be responsible for all correspondences and queries relating to this paper. KPN: Kali provides independent technical review, checking, guidance, critical suggestions with attention to details, editing and assist in the preparation of the manuscript.

Funding Open Access funding enabled and organized by CAUL and its Member Institutions.

Data availability All the data and models used during the present study appear in the published paper.

Declarations

Conflict of Interest The authors declare that there is no conflict of interest regarding the publication of this paper.

References

1. Atalar, C., Shin, E. C., & Das, B. M. (2009). Elastic modulus of granular soil-geogrid composite from cyclic plate load tests. *International Society for Soil Mechanic and Geotechnical Engineering*. https://doi.org/10.3233/978-1-60750-031-5-2212
2. Haas, R., Walls, J., & Carroll, R. G. (1988). Geogrid reinforcement of granular base in flexible pavements. 67th Annual Meeting, Transportation Research Board, Washington DC, USA.
3. Webster, S. L. (1993). Geogrid-reinforced base course for flexible pavements for light aircraft, test section construction, behaviour under traffic, laboratory tests, and design criteria, Technique Report GL-93-6, USAE Waterways Experiment Station, Vicksburg, MS.
4. Fannin, R. J., & Sigurdsson, O. (1996). Field observations on stabilisation of unpaved roads with geosynthetics. *Journal of Geotechnical Engineering, 122*(7), 544–553. https://doi.org/10.1061/(ASCE)0733-9410(1996)122:7(544)
5. Knapton, J., & Austin, R. A. (1996). Laboratory testing of reinforced unpaved roads. In H. Ochiai, N. Yasufuku, & K. Omine (Eds.), *Earth reinforcement* (pp. 615–618). Rottendam: Balkema.
6. Gabr, M. A., Leng, J., & Ju, T. J. (2001). *Response and characteristics of geogrid-reinforced aggregate under cyclic plate load* (p. 40). NC State University.
7. Leng, J., & Gabr, M. A. (2005). Numerical analysis of stress–deformation response in reinforced unpaved road sections. *Geosynthetics International, 2005*(12), 111–119. https://doi.org/10.1680/gein.2005.12.2.111
8. Al-Qadi, I. L., Dessouky, S. H., Kwon, J., Tutumluer, E. (2008). Geogrid in flexible pavements—validated mechanism. Transportation Research Record 2045, National Research Council, Washington DC, 102–109. doi: https://doi.org/10.3141/2045-12
9. Abu-Farsakh, M. Y., Gu, J., Voyiadjis, G. Z., & Chen, Q. (2014). Mechanistic–empirical analysis of the results of finite element analysis on flexible pavement with geogrid base reinforcement. *International Journal of Pavement Engineering, 15*, 786–798. https://doi.org/10.1080/10298436.2014.893315
10. Bagshaw, S. A., Herrington, P. R., Kathirgamanathan, P., & Cook, S. R. (2015). Geosynthetics in basecourse stabilisation. NZ Transport Agency research report 574, p. 64, ISBN 978-0-478-44577-0.
11. Chua, B. T., Hossam, A.-N., & Nepal, K. P. (2022). Analysis and design of geogrid-reinforced unbound granular pavement over soft subgrade for low volume roads. *Australian Geomechanics, 57*(1), 25–41.

12. Giroud, J. P., & Noiray, L. (1981). Geotextile-reinforced unpaved road design. Journal of the Geotechnical Division, ASCE, 107(9), Proceedings Paper 16489, 1233–1254. https://doi.org/10.1061/AJGEB6.0001187
13. Perkins, S. W., & Ismeik, M. (1997). A synthesis and evaluation of geosynthetic reinforced base course layers in flexible pavements: Part I experimental work. *Geosynthetics International, 4*(6), 549–604. https://doi.org/10.1680/gein.4.0106
14. Perkins, S. W., & Ismeik, M. (1997). A synthesis and evaluation of geosynthetic reinforced base course layers in flexible pavements: Part II analytical work. *Geosynthetics International, 4*(6), 605–621. https://doi.org/10.1680/gein.4.0107
15. Giroud, J. P., Ah-Line, C., & Bonaparte, R. (1984). *Design of unpaved roads and trafficked areas with geogrids*. Thomas Telford Publishing.
16. Milligan, G. W. E., & Love, J. P. (1984). Model testing of geogrids under an aggregate layer on soft ground. Proceedings, Symposium on Polymer Grid Reinforcement in Civil Engineering, Paper No. 4.2, London, England.
17. Giroud, J. P., & Han, J. (2004). Design method for geogrid-reinforced unpaved roads: I development of design method. *Journal of Geotechnical and GeoEnvironmental Engineering, 130*(8), 775–786. https://doi.org/10.1061/(ASCE)1090-0241(2004)130:8(787)
18. Giroud, J. P., & Han, J. (2004). Design method for geogrid-reinforced unpaved roads: II calibration and applications. *Journal of Geotechnical and GeoEnvironmental Engineering, 130*(8), 787–797. https://doi.org/10.1061/(ASCE)1090-0241(2004)130:8(787)
19. AASHTO 1993 (1993). Guide for design of pavement structures, American Association of State Highway and Transportation Officials, Washington DC, USA, ISBN: 1-56051-055-2.
20. Perkins, S. W., Christopher, B. R., Cuelho, E. L., Eiksund, G. R., Schwartz, C. S., & Svano, G. (2009). A M-E model for base-reinforced flexible pavements. *International Journal of Pavement Engineering, 10*(2), 101–114. https://doi.org/10.1080/10298430802009646
21. NCHRP (2004). Guide for mechanistic empirical design of new and rehabilitated pavement structures. Washington DC : National Cooperative Highway Research Program.
22. Perkins, S. W., Christopher, B. R., Lacina, B. A., & Klompmaker, J. (2012). M-E modelling of geosynthetic-reinforced unpaved roads. *International Journal of Geomechanics, 12*(4), 370–380. https://doi.org/10.1061/(ASCE)GM.1943-5622.0000184
23. Austroads (2009). Guide to pavement technology Part 4G: Geotextiles and Geogrids. Austroads Publication No. AGPT04/09, Sydney, NSW, ISBN: 978-1-921551-68-0.
24. Austroads (2019). Guide to pavement technology Part 2: Pavement Structural Design. Austroads Publication No. AGPT02–19, Sydney, NSW.
25. CIRCLY 7.0. User manual (2022). Mincad System Pty Ltd.
26. Christopher, B. R., & Wardle, L. (2013). Guidelines document on the use of CIRCLY to evaluate the benefits of geogrids for subgrade stabilisation in pavement structural design, Final Report.
27. DTMR (2018). Supplement to Part 2: Pavement Structural Design of the Austroads Guide to Pavement Technology. Queensland: Department of Transport and Main Roads.
28. RMS (2018). Supplement to Austroads Guide to Pavement Technology Part 2: Pavement Structural Design. New South Wales: Roads and Maritime Services.
29. Highways England (2020). Design of new pavement foundations, CD225, Highway England, Guildford, UK.
30. Highways England (2020). Design of new pavement constructions, CD226, Highway England, Guildford, UK.
31. Laboratoire Central des Ponts et Chaussées (1997). French design manual for pavement structures. Guide technique. Paris.
32. Austroads (2021). Technical basis of Austroads Guide to Pavement Technology Part 2: Pavement Structural Design. Austroads Publication No. AP-T356-21, ISBN 978-1-922382-721-9.
33. Austroads (2017). Guide to pavement technology Part 2: Pavement Structural Design. Austroads Publication No. AGPT02-17, Sydney, NSW, ISBN: 978-1-925854-69-5.
34. Priest, A. L., & Timm, D. H. (2006). Methodology and calibration of fatigue transfer functions for mechanistic-empirical flexible pavement design. National Centre for Asphalt Technology, NCAT Report 06-03. Auburn University.
35. HIPAVE 5.0 User manual (2022). Mincad System Pty Ltd.
36. Dorman, G. M., Edwards, J. M. (1964), Shell 1963 design charts for flexible pavements—an outline of their development. OPD Report No. 232/64M, Shell International Petroleum Company Limited.
37. Dorman, G. M., & Metcalf, C. T. (1965). Design curves for flexible pavements based on layered system theory. *Highway Research Record No., 71*, 69–84.
38. Dorman, G. M. (1962). The extension to practice of a fundamental procedure for the design of flexible pavements. Proc. Int. Conf. on Structural Design of Asphalt Pavements, Uni. of Michigan. 785–793.
39. Peattie, K. R. (1965) Design curves for flexible pavements based on layered system theory. Discussion, Highway Research Record, No. 71.
40. Heukelom, W., & Klomp, A. J. G. (1962). Dynamic testing as a means of controlling pavements during and after construction. Proc. Int. Conf. on the Structural Design of Asphalt Pavements, 667–679.
41. Monismith, C. L., & McLean, D. B. (1971). Design considerations for asphalt pavements. Institute of Transportation and Traffic Engineering, Univ. of California, Berkeley, Report TE 71-8.
42. Brown, S., & Brunton, J. (1984). Improvements to pavement subgrade strain criterion. *Journal of Transportation Engineering, ASCE, 110*(6), 551–567. https://doi.org/10.1061/(ASCE)0733-947X(1984)110:6(551)
43. Shell (1978). Shell pavement design manual—Asphalt pavements and overlays for road traffic. Shell International Petroleum Company Limited, London, UK.
44. Shell (1985). Addendum to the Shell pavement design manual. Shell International Petroleum Company Limited, London, UK.
45. Barker, W., & Brabston, W. (1975). Development of a structural design procedure for flexible airport pavements. Report No. S-75-17. US Army Corps of Engineers, Waterways Experiment Station, Vicksburg, Miss., USA. ISSN: 0360-859X.
46. Woodman, G. (1992). Failure criteria for flexible pavement. PSA report for BAA Technical Services Division, Surrey, UK.
47. Chou, Y. T., Development of failure criteria of flexible pavement thickness requirements for military roads and streets, elastic layered method. Department of the Army. Miscellaneous paper GL-92–1, 1992, p. 36.
48. Transport Research Laboratory (TRL) (1993). A guide to the structural design of bitumen-surfaced roads in tropical and subtropical countries. Overseas Road Note 31, 4th Edition, Overseas Centre, London, UK. ISSN: 0951-8797.
49. Pidwerbesky, B. D. (1995). Strain response and performance of subgrades and flexible pavements under various loading conditions. Transportation Research Record 1482, 87–93. ISSN: 0361-1981.
50. Corte, J. F., & Goux, M. T. (1996). Design of pavements structures: The French Technical Guide. *Transportation Research Record: Journal of the Transportation Research Board, 1539*, 116–124.

51. Wardle, L. J. & Roadway, B. (1998). Layered elastic design of heavy duty and industrial pavements. Proc. AAPA Pavement Industry Conf., Surfers Paradise, Australia, p. 9.
52. Huang, Y. H. (2004). *Pavement analysis and design* (2nd ed.). Pearson Prentice Hall. ISBN: 0131424734.
53. IRC:37-2012 (2012). Guidelines for the design of flexible pavements. Indian Roads Congress, New Delhi, India.
54. Gupta, A., Kumar, P., & Rastogi, R. (2014). M-E approach for design of low volume pavements. *International Journal of Pavement Engineering*. https://doi.org/10.1080/10298436.2014.960999
55. Claessen, A. I. M., Edwards, J. M., Sommer, P., & Uge, P. (1977). Asphalt pavement design, The Shell Method, Proceedings of the 4th International Conference on the Structural Design of Asphalt Pavements, Vol. 1, Ann Arbor, MI, 39–74.
56. Asphalt Institute (1982). Thickness design – asphalt pavements for highways and streets, Manual Series No. 1, 9th Edition, The Asphalt Institute, Lexington, Ky, USA, ISBN: 9781934154014.
57. Wardle, L. J., Rodway, B., Richards, I. (2001). Calibration of advanced flexible aircraft pavement design method to S77-1 method. In advancing aircraft pavements, ASCE, 2001 Aircraft Pavement Specialty Conference, Chicago, Illinois, 5–8 August 2001 (Buttlar, W.G. & Naughton, J.E. eds.), 192–201.
58. Rahman, M. D., Beecham, S., McIntyre, E., & Iqbal, A. (2018). Mechanistic design of concrete block pavements. Proceedings 2018 Australian Geomechanics Society Victoria Symposium. Geotechnics and Transport Infrastructure. Melbourne, Victoria, Australia, 13-17.
59. Pereira, A. T. (1977). Procedures for development of CBR design curves. Instruction Report S-77-1, US Army Corps of Engineers, Waterway Experiment Station, Vicksbury, Miss.
60. Austroads (1992). Pavement design: guide to the structural design of road pavements, (superseded) Austroads, Sydney, NSW, ISBN: 0855884010.
61. Austroads (2004). Pavement design: guide to the structural design of road pavements, AP-G17/04, (superseded) Austroads, Sydney, NSW, ISBN: 0855887028.
62. Vern, M. L., Dorè, G., Bilodeau, J. -P. (2016). Mechanistic-empirical design of unpaved roads. Conference of the Transportation Association of Canada, Toronto, ON.
63. Barksdale, R. D., Brown, S. F., Chan, F. (1989). Potential benefits of geosynthetics in flexible pavement systems. National Cooperative Highway Research Program Report 315, Transportation Research Board, Washington, D. C. p. 56.
64. Wathugala, G. W., Huang, B., & Pal, S. (1996). Numerical simulation of geosynthetic reinforced flexible pavement. *Transportation Research Record, 1534*, 58–65. https://doi.org/10.1177/0361198196153400109
65. Helwany, S., Dyer, J., & Leidy, J. (1998). Finite element analyses of flexible pavements. *Journal ofTransportation Engineering, 124*(5), 491–499. https://doi.org/10.1061/(ASCE)0733-947X(1998)124:5(491)
66. Howard, I., Warren, K. (2006). Finite element modelling approach for flexible pavements with geosynthetics, GeoCongress 2006: Geotechnical Engineering in the information Technology Age. Atlanta, GA. https://doi.org/10.1061/40803(187)234.
67. Ahirwar, S. K., & Mandal, J. N. (2017). Finite element analysis of flexible pavement with geogrids. *Procedia engineering, 189*, 411–416. https://doi.org/10.1016/j.proeng.2017.05.065
68. Duncan, J. M., Monismith, C. L., & Wilson, E. L. (1968). Finite element analyses of pavements, Highway Research Record 228, Highway Research Board, Washington DC, USA. 18–33.
69. Perkins, S. W. (2001). Numerical modeling of geosynthetic reinforced flexible pavements. Montana. Dept. of Transportation. Research Programs, p. 97, FHWA/MT-01-003/99160-2.
70. Perkins, S. W., & Edens, M. Q. (2002). Finite elements and distress models for geosynthetic-reinforced pavements. *International Journal of Pavement Engineering, 3*(4), 239–250. https://doi.org/10.1080/1029843021000083504
71. Saad, B., Mitri, H., & Poorooshasb, H. (2006). 3D FE Analysis of flexible pavement with geosythetic reinforcement. *Journal of Transportation Engineering, ASCE, 132*(5), 402–415. https://doi.org/10.1061/(ASCE)0733-947X(2006)132:5(402)
72. Abu-Farsakh, M. Y., & Nazzal, M. (2009). Evaluation of the base/subgrade soil under repeating loading: Phase 1—Laboratory testing and numerical modelling of geogrid-reinforced bases in flexible pavement, LTRC Project No. 05-5GT, Louisiana Department of Transportation and Development, Louisiana Transportation Research Centre, Baton Rouge, LA.
73. Moayedi, H., Kazemian, S., Prasad, A., Huat, B. K. (2009). Effect of geogrid reinforcement location in paved road improvement, Journal of Geotechnical Engineering. p. 11, http://www.ejge.com/2009/JourTOC14P.htm
74. Kim, M., Tutumluer, E., & Kwon, J. (2009). Nonlinear pavement foundation modeling for three-dimensional finite element analysis of flexible pavements. *International Journal of Geomechanics, ASCE*. https://doi.org/10.1061/(ASCE)1532-3641(2009)9:5(195)
75. Sahoo, U. C., & Reddy, K. S. (2010). Effect of nonlinearity in granular layer on critical pavement responses of low volume roads. *International Journal of Pavement Research and Technology, 3*(6), 320–325.
76. Gu, J. (2011). Computational modelling of geogrid-reinforced soil foundation and geogrid-reinforced base in flexible pavement, PhD Thesis, Louisiana State University and Agriculture and Mechanical College.
77. Austroads (2012). Development of a nonlinear finite element pavement response to load model, Austroads Publication No. AP-T199-12, Sydney, NSW, ISBN: 978-1-921991-24-0.
78. Pandey, S., Rao, K. R., & Tiwari, D. (2012). Effect of geogrid reinforcement on critical responses of bituminous pavements. 25th ARRB Conference. Perth, Australia p. 15.
79. Ghadimi, B., Nikraz, H., & Leek, C. (2013). Effects of geometrical parameters on numerical modelling of pavement granular material. *Airfield and Highway Pavement: Sustainable and Efficient Pavements, ASCE*. https://doi.org/10.1061/9780784413005.109
80. Kim, M. W., & Lee, J. H. (2013). Effects of geogrid reinforcement in low volume flexible pavement. *Journal of Civil Engineering and Management, 19*(Supplement 1), S14–S22. https://doi.org/10.3846/13923730.2013.793606
81. Faheem, H., & Hassan, A. M. (2014). 2D Plaxis finite element modelling of asphalt-concrete pavement reinforced with geogrid. *Journal of Engineering Sciences, 42*(6), 1336–1348. https://doi.org/10.21608/jesaun.2014.115106
82. Al-Jumaili, M. A. H. (2016). Finite element modelling of asphalt concrete pavement reinforced with geogrid by using 3D Plaxis software. *International Journal of Materials Chemistry and Physics, 2*(2), 62–70. ISSN:2394-7284.
83. Samb, F., Berthaud, Y., Ba, M., Fall, M., & Benboudjema, F. (2018). Nonlinear mechanical behaviour analysis of flexible laterite pavements of Senegal (West Africa) by FEM for M-E pavement design. *Geotechnical and Geological Engineering*. https://doi.org/10.1007/s10706-018-0514-y
84. Saad, B., Mitri, H., & Poorooshasb, H. (2005). Three-dimensional dynamic analysis of flexible conventional pavement foundation. *Journal of Transportation Engineering, ASCE, 131*(6), 460–469. https://doi.org/10.1061/(ASCE)0733-947X(2005)131:6(460)
85. Bodhinayake, B. B. (2008). A study on nonlinear behaviour of subgrades under cyclic loading for the development of a

design chart for flexible pavements. PhD Thesis, University of Wollongong.
86. Ghadimi, B. (2015). Numerical modelling for flexible pavement materials applying advanced finite element approach to develop Mechanistic-Empirical design procedure. PhD Thesis, University of Curtin.
87. SIMULIA (2014). ABAQUS Analysis User's Manual, Version 6.14. http://130.149.89.49
88. Lee, K. K., Cassidy, M. J., & Randolph, M. F. (2013). Bearing capacity on sand overlying clay soils: Experimental and finite element investigation of potential punch-through failure. *Geotechnique, 63*(15), 1271–1284. https://doi.org/10.1680/geot.12.P.175
89. Park, D., & Park, J. S. (2017). Capacity of bucket foundation on sand over clay layers, Proceedings of the 19th International Conference on Soil Mechanics and Geotechnical Engineering, Seoul 2325–2328. https://www.issmge.org/publications/online-library
90. Mosadegh, A., & Nikraz, H. (2015). Bearing Capacity Evaluation of Footing on a Layered-Soil using ABAQUS. *J Earth Sci Clim Change, 6*, 1000264.
91. Khodakarami, M. I., & Moghaddam, H. K. (2017). Evaluating the performance of rehabilitated roadway base with geogrid reinforcement in the presence of soil-geogrid-interaction. *Journal of Rehabilitation in Civil Engineering, 5*(1), 33–46. https://doi.org/10.22075/JRCE.2017.1299.1128
92. Look, B. G. (2014). *Handbook of geotechnical investigation and design tables*. CRC Press. ISBN: 9780203946602.
93. Ameratunga, J., Sivakugan, N., & Das, B. M. (2016). Correlations of soil and rock properties in geotechnical engineering. Developments in Geotechnical Engineering. New Delhi: Springer India, ISBN: 978-81-322-2629-1.
94. Manoharan, N., & Dasgupta, S. P. (1995). Bearing capacity of surface footings by finite elements. *Computers & Structures, 54*(4), 563–586. https://doi.org/10.1016/0045-7949(94)00381-C
95. Potts, D. M., Zdravković, L., Addenbrooke, T. I., Higgins, K. G., & Kovaćević, N. (2001). Finite element analysis in geotechnical engineering: Application. *Thomas Telford London*. https://doi.org/10.1680/feaigea.27831
96. Shiau, J. S., Lyamin, A. V., & Sloan, S. W. (2003). Bearing capacity of a sand layer on clay by finite element limit analysis. *Canadian Geotechnical Journal, 40*, 900–915. https://doi.org/10.1139/T03-042
97. Dondi, G. (1994). Three-dimensional finite element analysis of a reinforced paved road, 5th Int. Conf. on Geotextiles, Geomembranes and Related Products, Vol. 1, Singapore, 95–100.
98. Ling, H. I., & Liu, H. (2003). Finite element studies of asphalt concrete pavement reinforced with geogrid. *Journal of Engineering Mechanics, 129*(7), 801–811. https://doi.org/10.1061/(ASCE)0733-9399(2003)129:7(801)
99. Kwon, J., Tutumluer, E., & Konietzky, H. (2008). Aggregate base residual stresses affecting geogrid-reinforced flexible pavement response. *International Journal of Pavement Engineering, 9*, 275–285. https://doi.org/10.1080/10298430701582347
100. Leng, J., Ju, T. J., & Gabr, M. A. (2002). Characteristics of geogrid-reinforced aggregate under cyclic load. Transp. Res. Rec. Journal Transportation Research Board, 1786, 29–35. Transportation Research Board, National Research Council, Washington D C, USA.
101. Perkins, S. W., Christopher, B. R., Cuelho, E. L., & Eiksund, G. R. (2004). Development of design methods for geosynthetic reinforced flexible pavements. Report No. DTFH61-01-X-00068. U.S. Department of Transportation, Federal Highway Adminstration, Washington DC, USA.
102. Tang, X., Stoffels, S. M., & Palomino, A. M. (2016). Mechanistic-empirical approach to characterising permanent deformation of reinforced soft soil subgrade. *Geotextiles and Geomembranes, 44*, 429–441.
103. Perkins, S., & Cuelho, E. (1999). Soil-geosynthetic interface strength and stiffness relationships from pullout tests. *Geosynthetics International, 6*, 321–346. https://doi.org/10.1680/gein.6.0156
104. BOSTD (2007). Test Reports from TRI/Environmental Inc., Austin, Texas, USA.
105. Holz, R., Christopher, B. R., & Berg, R. R. (2008). Geosynthetic design and construction guidelines. Federal Highway Administration, Washington DC, USA.
106. South Africa Department of Transport (2009). Unsealed roads: Design, construction and maintenance. TRH 20, Pretoria, South Africa.
107. IRC:SP:72-2015 (2015). Guidelines for the design of flexible pavements for low volume rural roads. Indian Roads Congress, New Delhi, India.
108. Australia Road Research Board (2020). Unsealed Roads Best Practice Guide. https://www.arrb.com.au/bestpracticeguides
109. Wardle, L. J., Youdale, G., & Roadway, B. (2003). Current issues for mechanistic pavement design. 21st ARRB and 11th REAAA Conference, Cairns, Australia, 18–23 May 2003, Session S32, ARRB Transport Research.
110. Perkins, S. W. (2014). Modification of Austroads empirical design charts for paved roads reinforced with a NAUE geogrid. Final Report. Henning Ehrenberg NAUE GmbH & Co. KG. p. 30.
111. Cuelho, E., Perkins, S., & Morris, Z. (2014). Relative operational performance of geosynthetics used as subgrade stabilisation. Final project report FHWA/MT-14-002/7712-251. State of Montana, Department of Transportation.
112. DTMR (2017). Transport and Main Roads Specifications MRTS58 Subgrade Reinforcement using Pavement Geosynthetics. Technical Specification. Queensland: Department of Transport and Main Roads.
113. AASTHO (2017). Standard specification for geosynthetic specification for highway applications. American Association of State Highway and Transportation Officials. AASHTO Designation: M288-17.
114. Barksdale, R. G. (1971). Compressive stress pulse times in flexible pavements for use in dynamic testing. Highway Research Record 345, Highway Research Board, Washington DC, USA. 643–666. http://onlinepubs.trb.org/Onlinepubs/hrr/1971/345/345-003.pdf

Boon Tiong Chua is a fellow chartered professional engineer (FIEAust), KBR chief technical engineer (Civil), civil discipline manager and principal pavement engineer with over 43-year experience in construction and design consultancy in Department of Infrastructure and Transport, South Australia and overseas. Boon is a practising consulting civil engineer with a major focusing on pavement drainage, ground improvement, pavement technology, geosynthetic reinforcement, working platforms, numerical modelling of foundations and pavements.

Kali Prasad Nepal is a lecturer in civil engineering at Central Queensland University, Melbourne. His research focuses on experimental investigation and numerical modelling of foundations and pavements.